Springer

Journal of Mechanical Science and Technology 23 (2009) 1294~1305

Journal of Mechanical Science and Technology

www.springerlink.com/content/1738-494x
DOI 10.1007/s12206-009-0401-9

Micromechanically consistent calculation of rotational stiffness of radial tire †

Yong-Woo Kim*

Department of Mechanical Engineering, College of Engineering, Sunchon National University, Chonnam 540-742, Korea

(Manuscript Received June 23, 2008; Revised January 9, 2009; Accepted March 2, 2009)

Abstract

The rotational stiffness of a radial tire is one of the most important structural properties of the sidewall, and it has been evaluated conventionally by using a simplified model. However, in this paper, it is found that the conventional shear modulus used for the calculation of the stiffness is not micromechanically consistent. We examine the conventional shear modulus of the sidewall from the viewpoint of micromechanics, and present a new micromechanically consistent shear modulus for evaluating the rotational stiffness attributed to the shear deformation of sidewall. The developed method is discussed and rationalized through an approximate quantitative analysis. The calculation based on the micromechanically consistent shear modulus is validated by comparing it with experimental stiffness and the conventionally-calculated stiffness.

Keywords: Radial tire; Rotational stiffness; Sidewall; Carcass cord; Macroscopic shear modulus; Micromechanics; Tsai equation; Halpin-Tsai equation

1. Introduction

Modern tire structures have evolved through a series of modifications of the original pneumatic rubber tire. Early modifications were based on field experiences and on mostly experimental studies of tire behavior. The use of mathematical analysis to calculate tire stresses and deformations remained limited in scope for a long time because of the complexity of tire structure [1, 2]. Thus, many studies have used a simplified tire model, the "spring bedded ring model", which consists of the sidewall and tread. This simplified model has been used effectively since 1954 when Fiala [3] gave an explicit formula for cornering characteristics of a running tire. It has been applied to investigations on riding comfort [4], vibration [5-10], standing wave phenomena [11, 12], contact pressure distribution [13], and rolling resistance [14].

Akasaka et al. [15] gave an analytical method for estimating the rotational stiffness of a radial tire. They presented two analyses: the in-plane shear deformation theory and the netting theory. According to the netting theory, the rotational stiffness consists of two parts: one proportional to inflation pressure that causes cord tension, and the other attributed to the rubber rigidity of the sidewall. However, they explained neither how the conventional shear modulus of the latter stiffness was obtained from the viewpoint of micromechanics, nor why the shear rigidity of the cords packaged by rubber compound was ignored.

Kim et al. [16] explained why the shear rigidity of cords could be neglected in the conventional shear modulus of the sidewall by expressing it in terms of its respective material properties. They exemplified how to calculate it. Their calculation makes it possible to relate the rotational stiffness to the mechanical properties and geometrical dimensions of rubber compounds, so that the stiffness could be predicted.

Kim [17] proposed a new sidewall contour equa-

† This paper was recommended for publication in revised form by Associate Editor Jeong Sam Han

*Corresponding author. Tel.: +82 61 750 3536, Fax.: +82 61 750 3530
E-mail address: kyw@sunchon.ac.kr

tion, which is a deformable configuration of sidewall depending on applied torque, to calculate rotational stiffness of the part proportional to inflation pressure. He showed that the new sidewall contour equation could describe the real contour more precisely and easily than the conventional one and it gives improved rotational stiffness.

We consider the macroscopic shear modulus of the sidewall, showing that the shear modulus, which is used in References [15-17], is not inherently compatible with the real structure of the sidewall even if the rotational stiffness based on it gives an acceptable value to some degree. This paper presents a micromechanically consistent shear modulus. It calculates the rotational stiffness based on the new shear modulus as well as the conventional one to validate the newly defined shear modulus. The comparison between the rotational stiffnesses and the experimental one shows the micromechanically consistent calculation gives much closer stiffness to the experimental one than that calculated in a conventional way.

2. Rotational stiffness

When a tire fixed along the periphery of the tread is subjected to an applied torque T as shown in Fig. 1, the rotational stiffness of the sidewall is defined as

$$R = T/\psi \tag{1}$$

Assume that the sidewall under inflation pressure is a composite toroidal membrane structure that is composed of fiber-reinforced laminates with rubber compound matrix. Then we can assume that the applied torque supports the torque attributed to the cord tension and the torque caused by shear rigidity of the sidewall, that is, the applied torque can be written as [16, 17]

$$T = T(c) + T(s) \tag{2}$$

where $T(c)$ is the torque due to the tension of the carcass cords and $T(s)$ is the torque attributed to the shear rigidity of the sidewall.

From Eq. (1) and Eq. (2),

$$R = \frac{T(c) + T(s)}{\psi} = R(c) + R(s) \tag{3}$$

where $R(c) = T(c)/\psi$ and $R(s) = T(s)/\psi$.

In this paper, we calculated the part of $R(c)$ in the same manner as Reference [15] but not the part of $R(s)$. References [15]-[17] have assumed that the laminates in the sidewall are connected in series, which contradicts the real structure of the sidewall. We consider the shear modulus from the viewpoint of micromechanics and present a micromechanically consistent shear modulus of the sidewall.

Not to repeat the same analysis done in the previous papers here, we will quote only the equations needed to describe the present issue on $R(s)$.

2.1 Rotational stiffness due to shear deformation

Applying the in-plane shear deformation theory to a differential element of the sidewall shown in Fig. 2 and Fig. 3, we can obtain the rotational stiffness $R(s)$ given by [16, 17]

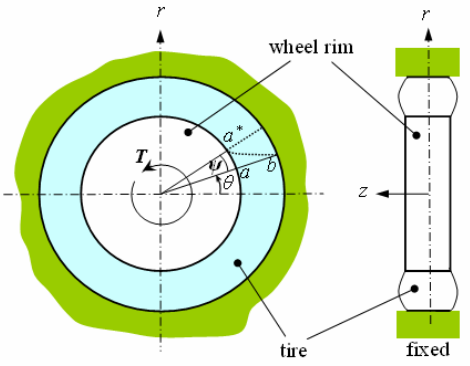

Fig. 1. Applied torque T and the rotational angle ψ; the line before deformation ab becomes a^*b after deformation.

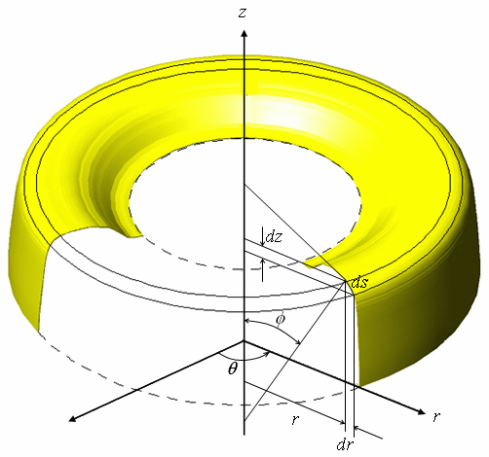

Fig. 2. A differential length of ds before deformation.

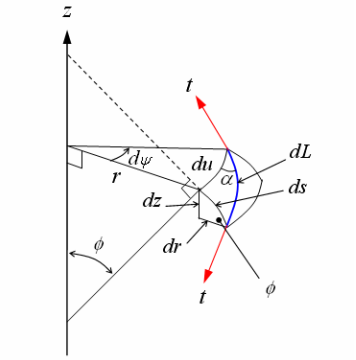

Fig. 3. The cord on a toroidal surface, where ds and dL are differential lengths before and after angular deformation ($d\psi$), respectively, and du is a circumferential displacement, α is cord angle, and t is the cord tension due to inflation pressure.

$$R(s)=\frac{T(s)}{\psi}=\frac{1}{\int_{r_B}^{r_D}\frac{1}{4\pi\, r^3\cos\phi\, G_{eq}h}dr}. \tag{4}$$

where

$$\cos\phi=\frac{\sqrt{\left\{(r_D)^2-(r_C)^2\right\}^2-\frac{\left\{r^2-(r_C)^2\right\}^2(\sin\phi_D)^2r^2(\sin\alpha_D)^2}{r^2-(r_D\cos\alpha_D)^2}}}{(r_D)^2-(r_C)^2}.. \tag{5}$$

It should be noted that G_{eq} in Eq. (4) is the macroscopic shear modulus of sidewall in the $\phi-\theta$ plane.

References [15]-[17] have defined the macroscopic shear modulus, G_{eq} as

$$G_{eq}=\frac{G_{rubber\ \ compounds}}{V_{rubber\ \ compounds}} \tag{6}$$

where $V_{rubber\ \ compounds}$ is the volume fraction of all the rubber compounds in the sidewall, i.e.,

$$V_{rubber\ \ compounds}=V_{sidewall}+V_{apex}+V_{innerliner}+V_{cm} \tag{7}$$

and $G_{rubber\ \ compounds}$ is the equivalent shear modulus of all the rubber compounds.

2.2 Review of the macroscopic shear modulus

The macroscopic shear modulus, G_{eq} in Eq. (6) corresponds to the shear modulus of the sidewall whose constituent rubber sheets and the carcass ply are connected in series. However, the definition of Eq. (6) contradicts the micromechanical behavior of laminates because the constituents are connected in parallel as shown in Fig. 4. To examine the above facts theoretically, we will consider four kinds of modeling of the sidewall.

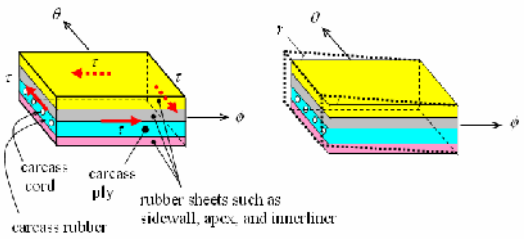

(a) (b)

Fig. 4. A representative volume element of sidewall composed of carcass ply and other rubber sheets; (a) shear stress τ , and (b) shear strain γ .

2.2.1 Model 1

If we assume the constituent rubber sheets and carcass ply are connected in parallel as shown in Fig. 5(a) and the carcass ply is modeled as shown in Fig. 5(b), we have

$$G_{eq}=V_{apex}G_{apex}+V_{sidewall}G_{sidewall}+V_{innerliner}G_{innerliner}+V_{cm}G_{cm}+V_{cf}G_{cf}. \tag{8}$$

The above equation can be expressed as

$$G_{eq}=V_{rubber\ \ compounds}G_{rubber\ \ compounds}+V_{cf}G_{cf} \tag{9}$$

If $G_{rubber\ \ compounds}=\frac{1}{V_{rubber\ \ compounds}}(V_{apex}G_{apex}+V_{sidewall}G_{sidewall}+V_{innerliner}G_{innerliner}+V_{cm}G_{cm})$. (10)

If all the rubber compounds have the same shear modulus, then Eq. (10) is reduced to Eq. (7) but Eq. (9) is different from Eq. (6). This means that the conventional definition of G_{eq} in Eq. (6) is not based on this model.

2.2.2 Mode 2

Once again, assume that the constituent rubber sheets of the sidewall and the carcass ply are connected in parallel as shown in Fig. 5(a). But if we model the carcass ply as shown in Fig. 5(c), then we have

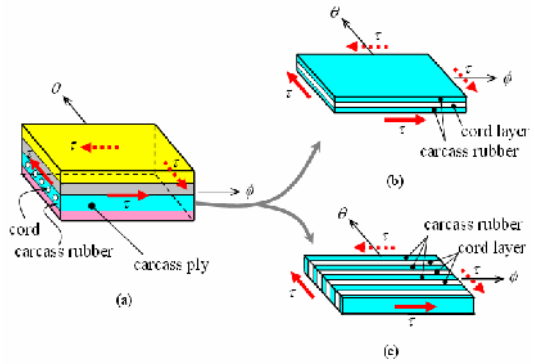

Fig. 5. (a) parallel-connection of rubber sheets and carcass ply, (b) assumption of parallel-connection of cords and carcass rubber in the carcass ply, and (c) assumption of series-connection of cords and carcass rubber in the carcass ply.

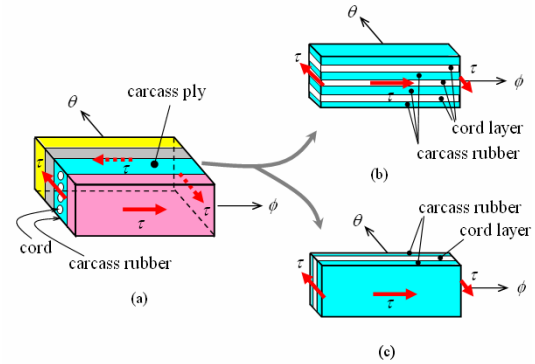

Fig. 6. (a) series-connection of rubber sheets and carcass ply, (b) assumption of parallel-connection of cords and carcass rubber in the carcass ply, and (c) assumption of series-connection of cords and carcass rubber in the carcass ply.

$$G_{eq} = V_{apex}G_{apex} + V_{sidewall}G_{sidewall} + V_{innerliner}G_{innerliner} + V_{carcass\ ply}\frac{1}{\frac{v_{cm}}{G_{cm}} + \frac{v_{cf}}{G_{cf}}} . \quad (11)$$

Since $v_{cf}/G_{cf} << v_{cm}/G_{cm}$, the above Eq. (11) can be written as

$$G_{eq} \approx V_{apex}G_{apex} + V_{sidewall}G_{sidewall} + V_{innerliner}G_{innerliner} + V_{carcass\ ply}\frac{G_{cm}}{v_{cm}} . \quad (12)$$

Eq. (12) can be rewritten as

$$G_{eq} \approx V_{rubber\ componds}G_{rubber\ compounds} \quad (13)$$

If $G_{rubber\ compounds} = \frac{1}{V_{rubber\ compounds}}(V_{apex}G_{apex} + V_{sidewall}G_{sidewall} + V_{innerliner}G_{innerliner} + V_{carcass\ ply}G_{cm}/v_{cm})$. (14)

If all the rubber compounds have the same shear modulus, then Eq. (14) is reduced to

$$V_{rubber\ compounds} = V_{sidewall} + V_{apex} + V_{innerliner} + V_{carcass\ ply}/v_{cm} \quad (15)$$

which is different from Eq. (7). Moreover, Eq. (13) is different from Eq. (6). This indicates that the conventional definition of G_{eq} in Eq. (6) is not based on this model.

2.2.3 Model 3

Assume that the constituent rubber sheets are connected in series as shown in Fig. 6(a) and the carcass-ply is modeled as shown in Fig. 6(b). Then the macroscopic shear modulus of the sidewall, G_{eq} can be written as

$$G_{eq} = \frac{1}{\frac{V_{aoex}}{G_{apex}} + \frac{V_{sidewall}}{G_{sidewall}} + \frac{V_{innerliner}}{G_{innerliner}} + \frac{V_{carcass\ ply}}{v_{cm}G_{cm} + v_{cf}G_{cf}}} . \quad (16)$$

Since $G_{cf} >> G_{cm}$, G_{apex}, $G_{sidewall}$, or $G_{innerliner}$ in fact, Eq. (16) can be rewritten as

$$G_{eq} \approx \frac{1}{\frac{V_{apex}}{G_{apex}} + \frac{V_{sidewall}}{G_{sidewall}} + \frac{V_{innerliner}}{G_{innerliner}}} . \quad (17)$$

The above equation is expressed as

$$G_{eq} \approx \frac{1}{V_{rubber\ compounds}/G_{rubber\ compounds}} = \frac{G_{rubber\ compounds}}{V_{rubber\ compounds}} \quad (18)$$

if $G_{rubber\ compounds} = \frac{1}{\frac{1}{V_{rubber\ compounds}}\left(\frac{V_{apex}}{G_{apex}} + \frac{V_{sidewall}}{G_{sidewall}} + \frac{V_{innerliner}}{G_{innerliner}}\right)}$. (19)

If all the rubber compounds have the same shear modulus, Eq. (19) is reduced to

$$V_{rubber\ compounds} = V_{sidewall} + V_{apex} + V_{innerliner} \quad (20)$$

which is slightly different from Eq. (7). This means that Eq. (6) is not based on this model. But note that the macroscopic shear modulus in Eq. (18) is quite similar to the conventional one in Eq. (6).

2.2.4 Model 4

Assume that the constituent rubber sheets are connected in series as shown in Fig. 6(a), which is not coincident with the real structure. Additionally, if we model the carcass ply as shown in Fig. 6(c), the G_{eq} can be written as

$$G_{eq} = \frac{1}{\frac{V_{aoex}}{G_{apex}} + \frac{V_{sidewall}}{G_{sidewall}} + \frac{V_{innerliner}}{G_{innerliner}} + \frac{V_{cm}}{G_{cm}} + \frac{V_{cf}}{G_{cf}}}. \quad (21)$$

The above equation can be rewritten as

$$G_{eq} = \frac{1}{\frac{V_{rubber\ compounds}}{G_{rubber\ compounds}} + \frac{V_{cf}}{G_{cf}}} \quad (22)$$

if $G_{rubber\ compounds} = \frac{1}{\frac{1}{V_{rubber\ compounds}}\left(\frac{V_{apex}}{G_{apex}} + \frac{V_{sidewall}}{G_{sidewall}} + \frac{V_{innerliner}}{G_{innerliner}} + \frac{V_{cm}}{G_{cm}}\right)}$. (23)

Since $V_{cf}/G_{cf} << V_{rubber\ compounds}/G_{rubber\ compounds}$, Eq. (22) can be written as

$$G_{eq} \approx \frac{G_{rubber\ compounds}}{V_{rubber\ compounds}}. \quad (24)$$

If all the rubber compounds have the same shear modulus, then Eq. (23) is reduced to Eq. (7). Moreover, Eq. (24) is approximately equal to Eq. (6). This indicates that the conventional modeling of the sidewall is based on this model. Thus, we will call this model with Eq. (21) the 'conventional model' in this paper.

2.2.5 Summary on the four models

Attention should be paid to the fact that the real structure of sidewall is far from the conventional model, that is, the shear modulus of Eq. (6) is not a correct shear modulus of the sidewall structure.

Comparing Eq. (18) of Model 3 with Eq. (24) of Model 4, we see that the two models will yield a similar value of G_{eq}. However, since the magnitude of $V_{rubber\ compounds}$ of Model 3 is less than that of Model 4, it is expected the rotational stiffness based on Model 3 is slightly greater than that based on Model 4 or the Conventional model.

Since Eq. (16) of Model 3 and Eq. (21) of Model 4 are not consistent with the rule of mixtures, we will rule out the two models from further consideration. However, since Model 1 and Model 2 are compatible with the real structure as far as the connection between rubber sheets and carcass-ply concerned, we will consider if they are micromechanically consistent from the other viewpoint in the later sections.

3. Micromechanically consistent shear modulus of sidewall

In this section, we will introduce the micromechanically consistent shear modulus by using the Tsai equation. This model will be called 'Tsai model' in this paper. Performing an approximate quantitative analysis of G_{eq} of Model 1, Model 2 and Tsai model, we will show that only the two models (Model 2 and Tsai model) are micromechanically consistent among them. Finally, we will present a generalized approximate expression of the micromechanically consistent G_{eq} by employing the Halpin-Tsai equation.

3.1 Shear modulus using the Tsai equation for carcass ply

Consider a representative volume element of sidewall that is subjected to shear stress τ caused by the torque $T(s)$ as shown in Fig. 4. If we assume that the representative sidewall element deforms according to $\tau = G_{eq}\gamma$ in a macroscopic sense, the equivalent shear modulus (G_{eq}) can be written as

$$G_{eq} = V_{apex}G_{apex} + V_{sidewall}G_{sidewall} + V_{innerliner}G_{innerliner} + V_{carcass\ ply}G_{carcass\ ply} \quad (25)$$

where $V_{[\bullet\bullet\bullet]}$ and $G_{[\bullet\bullet\bullet]}$ are volume fraction and

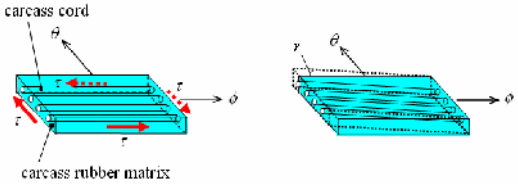

(a) (b)

Fig. 7. The volume element of carcass ply that is a part of the representative volume element of sidewall in Fig. 4; (a) shear stress τ, and (b) shear strain γ.

shear modulus of each constituent material written in the subscripts, respectively.

$G_{carcass\ ply}$ in Eq. (25) denotes the equivalent shear modulus of the carcass ply, which is composed of cords and rubber matrix as shown in Fig. 7. The $G_{carcass\ ply}$ can be expressed, by using the Tsai Eq. [18], as

$$G_{carcass\ ply} = (1-C)G_{cm}\frac{2G_{cf}-(G_{cf}-G_{cm})\nu_{cm}}{2G_{cm}+(G_{cf}-G_{cm})\nu_{cm}} + CG_{cf}\frac{(G_{cf}+G_{cm})-(G_{cf}-G_{cm})\nu_{cm}}{(G_{cf}+G_{cm})+(G_{cf}-G_{cm})\nu_{cm}} \quad (26)$$

where G_{cf} is the shear modulus of cord, G_{cm} is the shear modulus of carcass rubber matrix, ν_{cm} is the volume fraction of rubber compound within the carcass ply, and C denotes degree of contiguity of cords. Since the cords of the real tire under consideration are isolated from one another, we can assume that the value of C is zero. Then, the macroscopic shear modulus (G_{eq}) of the sidewall is given by

$$G_{eq} = V_{apex}G_{apex} + V_{sidewall}G_{sidewall} + V_{innerliner}G_{innerliner} + V_{carcass\ ply}G_{cm}\frac{2G_{cf}-(G_{cf}-G_{cm})\nu_{cm}}{2G_{cm}+(G_{cf}-G_{cm})\nu_{cm}} . \quad (27)$$

The above equation will be called the shear modulus of the 'Tsai model' in this paper.

3.2 Approximate quantitative analysis

Reconsider Model 1, Model 2 and Tsai model under the following assumption: Let G_{av} be the average value of the shear moduli of rubber compounds. Assume that the magnitude of each shear modulus of the rubber compounds is of the same order as that of G_{av} and the modulus of cord is much greater than G_{av}, i.e.,

$$G_{cf} >> G_{av} \approx G_{apex} \approx G_{sidewall} \approx G_{innerliner} \approx G_{cm} . \quad (28)$$

3.2.1 Mode 1

Dividing Eq. (8) by G_{av}, we have

$$\frac{G_{eq}}{G_{av}} = V_{apex}\frac{G_{apex}}{G_{av}} + V_{sidewall}\frac{G_{sidewall}}{G_{av}} + V_{innerliner}\frac{G_{innerliner}}{G_{av}} + V_{cm}\frac{G_{cm}}{G_{av}} + V_{cf}\frac{G_{cf}}{G_{av}} \quad (29)$$

Applying the condition in Eq. (28) to Eq. (29), we have

$$\frac{G_{eq}}{G_{av}} \approx V_{apex} + V_{sidewall} + V_{innerliner} + V_{cm} + V_{cf}\frac{G_{cf}}{G_{av}} = (1-V_{cf}) + V_{cf}\frac{G_{cf}}{G_{av}} . \quad (30)$$

Since $1-V_{cf} << V_{cf}\frac{G_{cf}}{G_{av}}$ for a real tire, the above Eq. (30) can be written as

$$\frac{G_{eq}}{G_{av}} \approx V_{cf}\frac{G_{cf}}{G_{av}} . \quad (31)$$

Hence, we have

$$G_{eq} \approx V_{cf}G_{cf} \quad (32)$$

which indicates that G_{eq} is roughly proportional to G_{cf}. This is not possible physically and we will exclude Model 1 from a further consideration. Note that Model 1 would give much higher macroscopic shear modulus than the conventional model of Model 4.

3.2.2 Mode 2

Division of Eq. (11) by G_{av} gives

$$\frac{G_{eq}}{G_{av}} = V_{apex}\frac{G_{apex}}{G_{av}} + V_{sidewall}\frac{G_{sidewall}}{G_{av}} + V_{innerliner}\frac{G_{innerliner}}{G_{av}} + V_{carcass\ ply}\frac{1}{\nu_{cm}\frac{G_{av}}{G_{cm}} + \nu_{cf}\frac{G_{av}}{G_{cf}}} \quad (33)$$

Applying the condition in Eq. (28) to Eq. (33), we have

$$\frac{G_{eq}}{G_{av}} \approx V_{apex} + V_{sidewall} + V_{innerliner} + V_{carcass\ ply}\frac{1}{\nu_{cm}} = V_{apex} + V_{sidewall} + V_{innerliner} + V_{carcass\ ply} + V_{carcass\ ply}\left(\frac{1}{\nu_{cm}}-1\right) = 1 + \frac{\nu_{cf}}{\nu_{cm}}V_{carcass\ ply} = 1 + \frac{V_{cf}}{V_{cm}}V_{carcass\ ply} . \quad (34)$$

3.2.3 Tsai model

Applying the condition in Eq. (28) to the Eq. (27) of the Tsai model, we have

$$\begin{aligned}\frac{G_{eq}}{G_{av}} &= V_{apex}\frac{G_{apex}}{G_{av}} + V_{sidewall}\frac{G_{sidewall}}{G_{av}} + V_{innerliner}\frac{G_{innerliner}}{G_{av}} \\ &\quad + V_{carcass\ ply}\frac{G_{cm}}{G_{av}}\frac{(2-\nu_{cm})\dfrac{G_{cf}}{G_{cf}} + \nu_{cm}\dfrac{G_{cm}}{G_{cf}}}{(2-\nu_{cm})\dfrac{G_{cm}}{G_{cf}} + \nu_{cm}\dfrac{G_{cf}}{G_{cf}}} \\ &\approx V_{apex} + V_{sidewall} + V_{innerliner} + V_{carcass\ ply}\frac{2-\nu_{cm}}{\nu_{cm}} \\ &= V_{apex} + V_{sidewall} + V_{innerliner} + V_{carcass\ ply}\left(1 + 2\frac{\nu_{cf}}{\nu_{cm}}\right) \\ &= 1 + 2\frac{\nu_{cf}}{\nu_{cm}}V_{carcass\ ply} \\ &= 1 + 2\frac{V_{cf}}{V_{cm}}V_{carcass\ ply}\ . \end{aligned} \tag{35}$$

Note that the above equation is quite analogous to Eq. (34).

3.3 Discussion of model 2 and Tsai model

To have an insight into Eq. (34) and Eq. (35), consider them by employing the Halpin-Tsai equation for $G_{carcass\ ply}$ as follows.

By using the Halpin-Tsai Eq. [18], $G_{carcass\ ply}$ in Eq. (25) is expressed as

$$G_{carcass-ply} = \frac{G_{cm}\left\{G_{cf}(1+\xi\nu_{cf}) + \xi G_{cm}(1-\nu_{cf})\right\}}{G_{cf}(1-\nu_{cf}) + \xi G_{cm}\left(1+\dfrac{\nu_{cf}}{\xi}\right)} \tag{36}$$

where ξ is a measure of fiber reinforcement of the composite that depends on fiber geometry, packing geometry, and loading condition.

Inserting Eq. (36) into Eq. (25) and assuming ξ is finite, we have

$$\begin{aligned}G_{eq} &= V_{apex}G_{apex} + V_{sidewall}G_{sidewall} + V_{innerliner}G_{innerliner} \\ &\quad + V_{carcass\ ply}\frac{G_{cm}\left\{G_{cf}(1+\xi\nu_{cf}) + \xi G_{cm}(1-\nu_{cf})\right\}}{G_{cf}(1-\nu_{cf}) + \xi G_{cm}\left(1+\dfrac{\nu_{cf}}{\xi}\right)}\end{aligned} \tag{37}$$

Applying the condition in Eq. (28) into Eq. (37), we obtain

$$\begin{aligned}\frac{G_{eq}}{G_{av}} &\approx V_{apex} + V_{sidewall} + V_{innerliner} + V_{carcass\ ply}\frac{1+\xi\nu_{cf}}{1-\nu_{cf}} \\ &= V_{apex} + V_{sidewall} + V_{innerliner} + V_{carcass\ ply} + V_{carcass\ ply}\frac{(1+\xi)\nu_{cf}}{1-\nu_{cf}} \\ &= 1 + (1+\xi)V_{carcass\ ply}\frac{\nu_{cf}}{\nu_{cm}} \\ &= 1 + (1+\xi)V_{carcass\ ply}\frac{V_{cf}}{V_{cm}}\ . \end{aligned} \tag{38}$$

It should be noted that Eq. (38) is equal to the Eq. (34) of Model 2 if $\xi = 0$, and Eq. (38) is identical to Eq. (35) of the Tsai model if $\xi = 1$. Therefore, Eq. (38) can be considered as a generalized approximate expression of the micromechanically consistent G_{eq} and thus Eq. (11) of Model 2 and Eq. (27) of Tsai model can be said to be micromechanically consistent in the sense of the approximate quantitative analysis.

Comparing Eq. (34) of Model 2 with Eq. (35) of Tsai model, we can predict that the rotational stiffness using Eq. (27) of Tsai model will be greater than that using Eq. (11) of Model 2.

4. How to calculate $R(s)$

Since G_{eq}, $\cos\phi$ and h in Eq. (4) are implicit functions of r, it is impossible to integrate Eq. (4) analytically. To calculate Eq. (4) by using numerical integration, we divide the sidewall into M ring-elements, which are axisymmetric about the z-axis as shown in Fig. 8 and Fig. 9. Fig. 8 is the cross-section of sidewall divided into M ring-elements by using the lines normal to the carcass cord line. Fig. 9(a) is the cross section of the k-th ring-element.

Fig. 9(a) shows the geometrical data such as the radial coordinates of intersections (r_k and r_{k+1}, $k = 1,2,...,M$) between carcass cord and the dividing lines, and the thicknesses ($\bar{h}_k$, $k = 1,2,...,M$) which are perpendicular to the carcass cord at $\bar{r}_k = \left(r_k + r_{k+1}\right)/2$. In Fig. 9(a), $A^{(k)}_{total}$ is the cross-sectional area of the k-th ring-element and $A^{(k)}_{[\bullet\bullet\bullet]}$ is the cross-sectional area of the constituent [$\bullet\bullet\bullet$] in the k-th ring element. The $\bar{r}^{(k)}_{[\bullet\bullet\bullet]}$ and $\bar{r}^{(k)}_{total}$ in Fig. 9(b) denote the distances from the z axis to the centroid of the areas $A^{(k)}_{[\bullet\bullet\bullet]}$ and $A^{(k)}_{total}$, respectively, along radial direction. Then we have

$$A^{(k)}_{total} = A^{(k)}_{sidewall} + A^{(k)}_{apex} + A^{(k)}_{carcass\ ply} + A^{(k)}_{innerliner}\ . \tag{39}$$

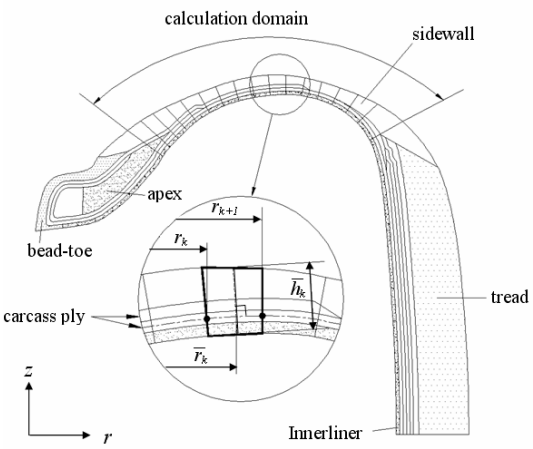

Fig. 8. Division of the calculation domain in the sidewall.

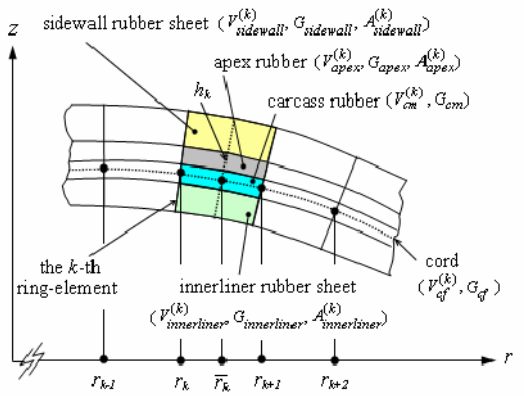

(a)

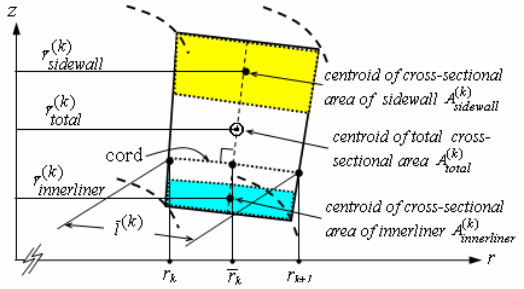

(b)

Fig. 9. Rubber sheets and carcass ply in the k -th ring-element of the sidewall.

Since the volumes of each sheet and ply in the k -th ring-element are axisymmetric about z -axis, they are calculated as follows. The volume of the k -th ring-element with cross-sectional area $A_{total}^{(k)}$ and its centroid at $r = \bar{r}_{total}^{(k)}$ is given by

$$Vol_{total}^{(k)} = 2\pi\, \bar{r}_{total}^{(k)}\, A_{total}^{(k)}. \tag{40}$$

In the same way, the constituent volumes in the k -th ring-element are defined by

$$Vol_{sidewall}^{(k)} = 2\pi\, \bar{r}_{sidewall}^{(k)}\, A_{sidewall}^{(k)} \quad \text{for the sidewall rubber sheet,} \tag{41}$$

$$Vol_{innerliner}^{(k)} = 2\pi\, \bar{r}_{innerliner}^{(k)}\, A_{innerliner}^{(k)} \quad \text{for the innerliner rubber sheet,} \tag{42}$$

$$Vol_{apex}^{(k)} = 2\pi\, \bar{r}_{apex}^{(k)}\, A_{apex}^{(k)} \quad \text{for the apex rubber,} \tag{43}$$

and

$$Vol_{caracss\ ply}^{(k)} = 2\pi\, \bar{r}_{carcass\ ply}^{(k)}\, A_{carcass\ ply}^{(k)} \quad \text{for the carcass ply.} \tag{44}$$

Then we have

$$Vol_{total}^{(k)} = Vol_{sidewall}^{(k)} + Vol_{carcass\ ply}^{(k)} + Vol_{apex}^{(k)} + Vol_{innerliner}^{(k)}. \tag{45}$$

The volume of carcass cord in the k -th ring-element is given by

$$Vol_{cf}^{(k)} = n\frac{\pi d^2}{4}\bar{l}^{(k)} \tag{46}$$

where n is the cord end count, d is the diameter of carcass cord , and $\bar{l}^{(k)}$ is the length of cord in the k -th ring-element. Then the volume of carcass rubber in the k -th ring-element is given by

$$Vol_{cm}^{(k)} = Vol_{carcass\ ply}^{(k)} - Vol_{cf}^{(k)}. \tag{47}$$

The values of $\bar{r}_{[\bullet\bullet\bullet]}^{(k)}$, $A_{[\bullet\bullet\bullet]}^{(k)}$ and $\bar{l}^{(k)}$ in Eqs. (40)-(46) are measured from the cross-section of the sidewall.

The volume fractions of the constituents in the k -th ring-element are defined as follows.

$$V_{sidewall}^{(k)} = Vol_{sidewall}^{(k)} / Vol_{total}^{(k)} \quad \text{for the sidewall rubber sheet,} \tag{48}$$

$$V_{innerliner}^{(k)} = Vol_{innerliner}^{(k)} / Vol_{total}^{(k)} \quad \text{for the innerliner rubber sheet,} \tag{49}$$

$$V_{apex}^{(k)} = Vol_{apex}^{(k)} / Vol_{total}^{(k)} \quad \text{for the apex rubber,} \tag{50}$$

and

$$V_{carcass\ ply}^{(k)} = Vol_{carcass\ ply}^{(k)} / Vol_{total}^{(k)} \quad \text{for the carcass ply.} \tag{51}$$

Additionally, the volume fraction of the carcass cord in the k -th ring-element is given by

$$V_{cf}^{(k)} = Vol_{cf}^{(k)} \Big/ Vol_{total}^{(k)} \tag{52}$$

and the volume fraction of the carcass rubber in the k -th ring-element is

$$V_{cm}^{(k)} = Vol_{cm}^{(k)} \Big/ Vol_{total}^{(k)} \ . \tag{53}$$

Thus we have

$$V_{sidewall}^{(k)} + V_{innerliner}^{(k)} + V_{apex}^{(k)} + V_{carcass\ ply}^{(k)} = 1 \tag{54}$$

and

$$V_{carcass-ply}^{(k)} = V_{cm}^{(k)} + V_{cf}^{(k)} \ . \tag{55}$$

Dividing the both sides of Eq. (55) by $Vol_{carcass\ ply}^{(k)}$, we have

$$v_{cm}^{(k)} + v_{cf}^{(k)} = 1 \tag{56}$$

where the volume fractions, $v_{cm}^{(k)}$ and $v_{cf}^{(k)}$ are defined as

$$v_{cm}^{(k)} = Vol_{cm}^{(k)} \Big/ Vol_{carcass\ ply}^{(k)} \tag{57}$$

and

$$v_{cf}^{(k)} = Vol_{cf}^{(k)} \Big/ Vol_{carcass\ ply}^{(k)} \ . \tag{58}$$

Using Eq. (27), the equivalent shear modulus of the k -th ring-element is given by

$$G_{eq}^{(k)} = V_{apex}^{(k)} G_{apex} + V_{sidewall}^{(k)} G_{sidewall} + V_{innerliner}^{(k)} G_{innerliner} + V_{carcass\ ply}^{(k)} G_{cm} \frac{2G_{cf} - (G_{cf} - G_{cm}) v_{cm}^{(k)}}{2G_{cm} + (G_{cf} - G_{cm}) v_{cm}^{(k)}} \tag{59}$$

where the shear moduli for apex rubber, sidewall rubber sheet, and innerliner rubber sheet are given by

$$G_{[\bullet\bullet\bullet]} = \frac{E_{[\bullet\bullet\bullet]}}{2(1+\mu_{[\bullet\bullet\bullet]})} \ . \tag{60}$$

In Eq. (60), $E_{[\bullet\bullet\bullet]}$ and $\mu_{[\bullet\bullet\bullet]}$ are Young's modulus and Poisson's ratio of the material [$\bullet\bullet\bullet$] in subscripts, respectively.

The rotational stiffness $R(s)$ using the Tsai model is calculated as follows. Employing Eq. (59) and numerical integration by the trapezoidal rule, we rewrite Eq. (4) as

$$R(s) = \frac{1}{\sum_{k=1}^{M} \dfrac{r_{k+1} - r_k}{4\pi(\overline{r}_k)^3 \cos\overline{\phi}_k G_{eq}^{(k)} \overline{h}_k}} \tag{61}$$

where

$$\overline{r}_k = \frac{r_k + r_{k+1}}{2} \ , \tag{62}$$

$$\cos\overline{\phi}_k = \frac{\sqrt{\left\{(r_D)^2 - (r_C)^2\right\}^2 - \dfrac{\left\{(\overline{r}_k)^2 - (r_C)^2\right\}^2 (\sin\phi_D)^2 (\overline{r}_k)^2 (\sin\alpha_D)^2}{(\overline{r}_k)^2 - (r_D\cos\alpha_D)^2}}}{(r_D)^2 - (r_C)^2} \tag{63}$$

and $\overline{h}_k$ is the thickness of the k -th ring-element at $r = \overline{r}_k$.

5. Numerical results and discussion

A radial tire of P205/60R15 is used to validate the present study. Its geometric parameters are $r_B = 222.0\ mm$, $r_C = 256.0\ mm$, $r_D = 283.84\ mm$ and $\phi_D = 54^o$ as shown in Fig. 10. The cord diameter $d = 0.6$ mm, and the cord end count $n = 1470$. All the necessary geometrical data including volume fractions are obtained directly from the tire geometry.

Young's modulus of each rubber sheet has been obtained from the tensile test, in which specimens are sampled from the real tire:

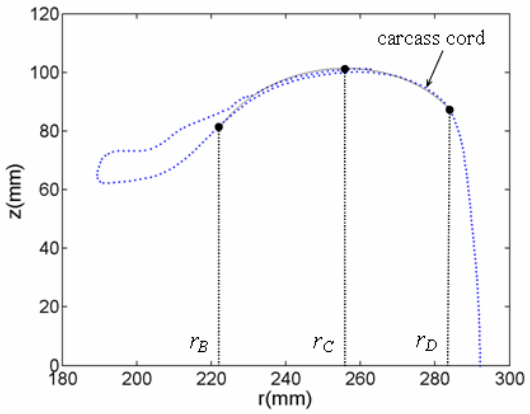

Fig. 10. Sidewall contour.

$E_{apex} = 24.14\ MPa$

$E_{sidewall} = 3.38\ MPa$

$E_{innerliner} = 4.52\ MPa$

$E_{cm} = 4.59\ MPa$

$E_{cf} = 7.13\ GPa$.

The above Young's moduli of rubber compounds are obtained by applying the Mooney-Rivlin function to the stress-strain curves in the range of strain of 0~0.05. For details about the preparation of specimens and test procedure refer to Reference [19].

Since the rubber compounds are nearly incompressible, their Poisson ratios are assumed as $\mu = 0.49$.

The values of rotational stiffness are different from each other, depending on the definitions of G_{eq} , i.e., Eqs. (8), (11), (16), (21) and (27). To find an optimal number of sidewall divisions, we performed a convergence test of the stiffnesses in terms of the number of ring-elements, which is plotted in Fig. 11. Employing the sidewall divided into 10 ring-elements, which produces nearly-converged stiffnesses except that of Model 1, we calculated the rotational stiffnesses $R = R(c) + R(s)$ and plotted them in Fig. 12 together with the experimental one [16].

Since the value of $R(c)$ is zero at the inflation pressure, $p = 0$, the rotational stiffness R at $p = 0$ is the same as $R(s)$. Since all of the $R(c)$ in the five models in Fig. 12 are calculated by using the same equation and the value of $R(s)$ in each model is constant irrespective of inflation pressure, the $\partial R/\partial p$ of the five models are identical.

The value of $R(s)$ based on Model 1 is too high, which was predicted in section 3.2.1. Even if the rotational stiffnesses based on Model 3 and Model 4, which are not micromechanically consistent, are close to the experimental one, they are fortuitous. The rotational stiffness based on Model 3 is greater than that based on Model 4 as we predicted in section 2.2.5.

The macroscopic shear moduli based on Model 2 and the Tsai model are micromechanically consistent in the sense of the approximate quantitative analysis. The rotational stiffness based on Tsai model is greater than that based on Model 2 as we predicted in section 3.3. Fig. 12 shows that both Model 2 and the Tsai model produce better approximations than the conventional model of Model 4.

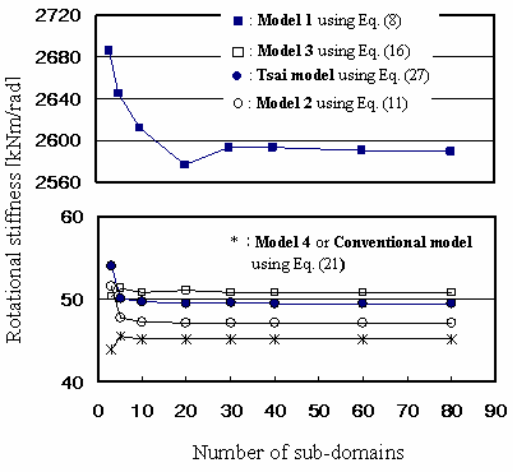

Fig. 11. Convergence test of rotational stiffnesses in terms of the number of ring-elements when $p = 210$ kPa .

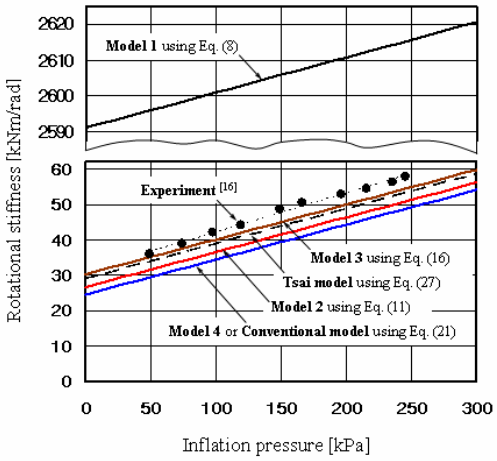

Fig. 12. Comparison of the rotational stiffnesses with experimental one.

6. Conclusions

The conventional calculation of rotational stiffness of radial tire consists of two parts: one part attributed to the cord tension due to inflation pressure and the other attributed to the shear rigidity of the sidewall. Focusing on the calculation of the latter, we have shown that the conventional macroscopic shear modulus of the sidewall is not micromechanically consistent even if it may give an acceptable rotational stiffness to some degree.

Modeling the sidewall in five ways, we have shown that Model 2 and the Tsai model provide a micromechanically consistent shear modulus of the sidewall.

The calculations based on the two models give enhanced results compared with the conventional calculation. We also have presented a generalized approximate expression of the macroscopic shear modulus of the sidewall by employing the Halpin-Tasi equation for carcass ply.

Nomenclature

α : Cord angle, Fig. 3
α_D : Cord angle at $r = r_D$
v_{cf} : Volume fraction of *cf* within carcass ply
v_{cm} : Volume fraction of *cm* within carcass ply
ϕ : Meridian angle, Fig. 2 and Fig. 3
ϕ_D : Meridian angle at $r = r_D$
ψ : Rotational angle of rim, Fig. 1
r_B, r_C, r_D : r-coordinates, Fig. 10
r, θ, z : Coordinates, Fig. 1 and Fig. 2
G_{eq} : Macroscopic shear modulus of sidewall
$G_{[\bullet\bullet\bullet]}$: Shear modulus of the material in bracket
T : Applied torque, Fig. 1
$T(c)$: Torque owing to the tension of carcass cords
$T(s)$: Torque attributed to the shear rigidity of sidewall
R : Rotational stiffness of sidewall
$R(c)$: Rotational stiffness owing to the tension of carcass cords
$R(s)$: Rotational stiffness attributed to the shear rigidity of sidewall
$V_{[\bullet\bullet\bullet]}$: Volume fraction of the material in bracket

Subscripts

cf : Cords of carcass ply
cm : Rubber matrix of carcass ply

References

[1] E. Robecchi and L. Amichi, Mechanics of the inflated tire, *Tire Science and Technology*, 1 (3) (1973) 290-345.
[2] R. H. Kennedy, H. P. Patel and M. S. McMinn, Radial truck tire inflation analysis: theory and experiment, *Rubber Chemistry and Technology*, 54 (1982) 751-766.
[3] E. Fiala, Seitenkraft am rollenden Luftreifen, *Z. VDI*, 96 (26) (1954) 937-979.
[4] M. Takayama and K. Yamagishi, Simulation model for tire vibration, *Tire Science and Technology*, 11 (1) (1984) 38-49.
[5] J. T. Tielking, Plane vibration characteristics of a pneumatic tire model, *SAE* 650492 (1965).
[6] G. R. Potts, C. A. Bell, L. T. Charek and T. K. Roy, Tire vibrations, *Tire Science and Technology*, 5 (4) (1977) 202-225.
[7] T. Kamitamari and H. Sakai, A study on radial tire vibration, *SAE* 852185 (1985) 153-158.
[8] S. C. Huang and W. Soedel, Effect of Coriolis acceleration on the free and forced in-plane vibrations of rotating rings on elastic foundation, *Journal of Sound and Vibration*, 115 (2) (1987) 253-274.
[9] H. Pacejka, Tire in-plane dynamics, in *Mechanics of Pneumatic Tires* edited by Clark, S. K., (1981) 726-784.
[10] C. R. Dohrmann, Dynamics of a tire-wheel-suspension assembly, *Journal of Sound and Vibration*, 205 (5) (1998) 627-642.
[11] J. Padovan, On viscoelasticity and stand waves in tires, *Tire Science and Technology*, 4 (4) (1976) 233.
[12] A. Chatterjee, J. P. Cusumano and J. D. Zolock, On contact-induced standing waves in rotating tires: experiment and theory, *Journal of Sound and Vibration*, 227 (5) (1999) 1049-1081.
[13] J. Jenkins, The circumferential contact problem for the belted radial passenger car tire, *Vehicle System Dynamics*, 11 (1982) 325-343.
[14] D. S. Stutts and W. Soedel, A simplified dynamic model of the effect of internal damping on the rolling resistance in pneumatic tires, *Journal of Sound and Vibration*, 155 (1) (1992) 153-164.
[15] T. Akasaka, S. Yamazaki and K. Asano, An approximate evaluation of rotational stiffness of radial tire, *Transactions of JSCM*, 10 (1) (1984) 24-31.
[16] Y.-W. Kim and Y. Kim, New evaluation and test of sidewall's rotational stiffness of radial tire, *Journal of Mechanical Science and Technology*, 20 (6) (2006) 748-758.
[17] Y.-W. Kim, New sidewall contour for evaluation of sidewall's rotational stiffness of a radial tire, *Journal of Mechanical Science and Technology*, 22 (1) (2008) 2-11.
[18] R. M. Jones, *Mechanics of Composite Materials.* McGraw-Hill Book Company, (1975).
[19] Y.-W. Kim and J. G. Kim, Calculation of sidewall lateral stiffness of a radial tire using material properties of rubber compounds, *Transactions of the Korean Society of Mechanical Engineers*, A (10) (2003) 1667-1675.

Yong-Woo Kim received his Bachelor degree in Mechanical Engineering from Yonsei University, Seoul, Korea, in 1982, and his Ph.D. degree from Yonsei Graduate School in 1991. Dr. Kim is currently Professor at Department of Mechanical Engineering at Sunchon National University in Sunchon, Korea. Dr. Kim's research interests include structural analysis, machine design, and tire mechanics.